Intrazeolite Chemistry of Nickel(0) Complexes and Ni(0,II) Clusters Studied by EXAFS, Solid-State NMR, and FT-IR Spectroscopy

Thomas Bein,*[1a,b] Stephan J. McLain,*[1a] David R. Corbin,[1a] Rodney D. Farlee,[1a] Karin Moller,[1a,b] Galen D. Stucky,[1a,c] Geoffrey Woolery,*[1d] and Dale Sayers[1e]

Contribution from the Central Research and Development Department,† E. I. du Pont de Nemours and Company, Experimental Station, Wilmington, Delaware 19898, the Paulsboro Research Laboratory, Mobil Research and Development Corporation, Paulsboro, New Jersey 08066, and the Department of Physics, North Carolina State University, Raleigh, North Carolina 27695. *Received March 3, 1987*

Abstract: Adsorption, thermal decomposition, and reactivity of $Ni(CO)_4$ in the cage system of dehydrated zeolite Y has been studied with EXAFS and near-edge spectroscopies, in particular monitoring changes in oxidation states and Ni ligation. $Ni(CO)_4$ is adsorbed as an intact molecule in cation-free zeolite Y, LiY, and NaY. Symmetry changes of the molecule in LiY and NaY are assigned to the formation of cation--OC-Ni bridges. Thermal treatment of the $Ni(CO)_4$/NaY adduct leads to loss of CO concomitant with the formation of a bimodal Ni phase. A major part of the Ni forms small clusters (approximately 0.5 to 1.5 nm), in addition to larger crystallites (5-30 nm), sticking at the outer surface of the zeolite crystals. Oxidation of $Ni(CO)_4$/NaY to NiO/NaY with molecular oxygen occurs almost to completion below 295 K. The small NiO particles are stable to sintering up to 670 K. Nickel-phosphine/NaY adducts have been prepared by direct adsorption from solution [$Ni(CO)_3PMe_3$, $Ni(CO)_2(PMe_3)_2$], and by synthesis inside the NaY supercage [$Ni(CO)_3PMe_3$, $Ni(CO)_3(PPh_2CHMe_2)$, $Ni(CO)_3P(t\text{-}Bu)_3$, $Ni(PMe_3)_x$]. The NaY/$Ni(CO)_3(PPh_2CHMe_2)$ adduct is a ship-in-a-bottle complex, i.e., the Ni complex is too large to exit the zeolite supercage. The substitution of carbonyl ligands by phosphines was monitored in the near-edge and EXAFS modulations as well as with ^{31}P MAS NMR. EXAFS is an excellent method to monitor ligand coordination and provides information that is complimentary to IR spectroscopy.

The interplay between organometallic molecules and oxide surfaces has attracted growing attention during the last decade. A major incentive to study these systems is to anchor catalytically active species on heterogeneous supports for the purpose of facile recovery from the reaction mixture.[2] Homogeneous catalysts, if immobilized for instance in the cage system of zeolites, might be expected to be stabilized against aggregation or bimolecular deactivation. Furthermore, the zeolite cage system may favor unique selectivity of a catalytic reaction due to changed complex geometries, transition-state modifications, and/or diffusional selectivity for the substrate molecules.

Thermal decomposition of supported $Ni(CO)_4$ as a precursor for dispersed Ni catalysts[3-7] and a limited number of attempts to anchor mixed $Ni(CO)_nL_m$ complexes directly on partially hydroxylated oxide surfaces[8,9] have been reported previously.

The reaction of $Ni(CO)_4$ with NaX zeolite, its thermal stability, and the generation of encapsulated phosphine complexes have recently been studied with IR techniques.[10] The effect of pore blocking at high loading densities and selectivity for ligands of certain size have been demonstrated. The limitations of IR spectroscopy for these systems prevented a definitive identification of the reaction products.

A major challenge for research on supported metal systems is the detailed characterization of the metal environment. In an attempt to understand the behavior of nickel carbonyl compounds in the cage system of faujasites, we have used a combination of EXAFS and X-ray absorption near edge spectroscopy, complemented by ^{31}P MAS-NMR and FT-IR experiments.

Results and Discussion

1. Adsorption of $Ni(CO)_4$ in Faujasite. Zeolites NaY and dealuminated Y (with Si/Al > 400, hereafter referred to as Y*) readily adsorb $Ni(CO)_4$ vapor to give saturated samples with compositions NaY$\langle Ni(CO)_4\rangle_{3.9}$ and Y*$\langle Ni(CO)_4\rangle_{2.9}$ (i.e., 3.9 and 2.9 Ni per supercage). The lower adsorption capacity of Y* may be due to lower crystallinity, or pore blocking by non-framework Al. These saturated zeolites were unstable with respect to loss of $Ni(CO)_4$; they frequently formed Ni mirrors in the sample vials. Because of this instability, most spectroscopic characterization was one on samples with lower $Ni(CO)_4$ loadings.

Infrared spectra of $Ni(CO)_4$ in Y*, NaY, and LiY show striking differences (Figures 1-3). The single carbonyl band observed in Y* (2046 cm^{-1}, Figure 1B,C) resembles the spectrum of $Ni(CO)_4$ in THF solution (Figure 1A). NaY$\langle Ni(CO)_4\rangle_{0.22}$ has four carbonyl bands at 2132, 2072, 2033, and 2000 cm^{-1} (Figure 2A). At a loading of 2.2 Ni per supercage, the bands are not as well resolved and the 2072-cm^{-1} band has shifted to 2066 cm^{-1} (Figure 2B). In LiY the spectrum changes dramatically as the Ni loading is increased. With 0.25 Ni per supercage, the spectrum resembles NaY$\langle Ni(CO)_4\rangle_{0.22}$ with four bands at 2129, 2068, 2033, and 1996 cm^{-1} (Figure 3A). With 2.0 Ni per supercage, the minor band at 2044 cm^{-1} increases to become the largest band in the spectrum (Figure 3B).

$Ni(CO)_4$ can be displaced from NaY$\langle Ni(CO)_4\rangle_x$ by washing with THF. After a Ni-zeolite sample is stirred for 18 h in THF, all of the $Ni(CO)_4$ is found in the THF solution. The polar THF must be more strongly adsorbed than nonpolar $Ni(CO)_4$.

Previous IR studies of metal carbonyls in zeolites suggested labilization of carbonyl ligands to give small metal clusters and metal subcarbonyls.[11] For example, the generation of yellow/

† Contribution No. 4257.

(1) (a) E. I. du Pont de Nemours and Company. (b) Current address: Department of Chemistry, University of New Mexico, Albuquerque, NM 87131. (c) Current address: Department of Chemistry, University of California, Santa Barbara, CA 93106. (d) Mobil Research and Development Corporation. (e) North Carolina State University.

(2) Bailey, D. C.; Langer, S. H. *Chem. Rev.* **1981**, *81*, 109.
(3) Galich, P. N.; Gutyryra, V. S.; Galinski, A. A. *Proceedings of the 5th International Zeolite Conference*; Rees, L. V. C., ed.; Heyden: London, 1980; p 661.
(4) Derouane, E. G.; Nagy, J. B.; Vedrine, J. C. *J. Catal.* **1977**, *46*, 434.
(5) Bjorklund, R. B.; Burwell, R. L., Jr. *J. Colloid Interface Sci.* **1979**, *70*, 383.
(6) Hucul, D. A.; Brenner, A. *J. Phys. Chem.* **1981**, *85*, 496.
(7) Hucul, D. A.; Brenner, A. *J. Am. Chem. Soc.* **1981**, *103*, 217.
(8) Tessier Youngs, C.; Correa, F.; Pioch, D.; Burwell, R. L.; Shriver, D. F. *Organometallics* **1983**, *2*, 898.
(9) Pierce, J. L.; Walton, R. A. *J. Catal.* **1983**, *81*, 375.
(10) Herron, N.; Stucky, G. D.; Tolman, C. A. *Inorg. Chim. Acta* **1985**, *100*, 135.
(11) Ballivet-Tkatchenko, D.; Coudurier, G. *Inorg. Chem.* **1979**, *18*, 558.

0002-7863/88/1510-1801$01.50/0

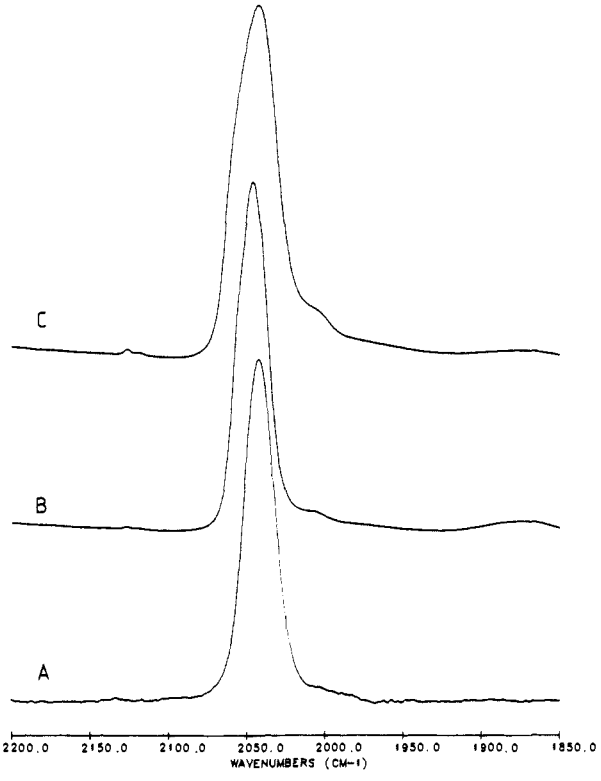

Figure 1. Infrared spectra of nickel tetracarbonyl in different environments at 295 K: (A) in THF solution; (B) in dealuminated Y* zeolite, 0.16 Ni per supercage; (C) in dealuminated Y* zeolite, 1.4 Ni per supercage.

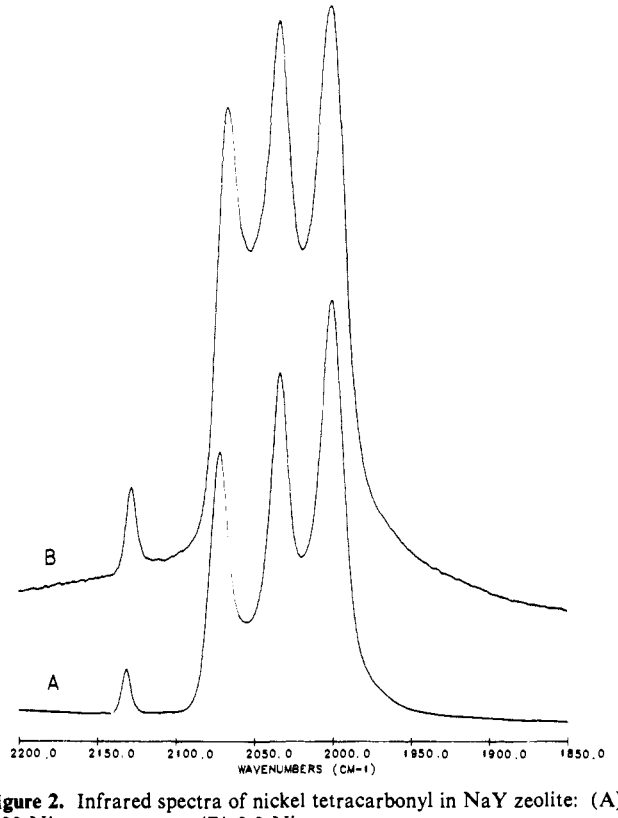

Figure 2. Infrared spectra of nickel tetracarbonyl in NaY zeolite: (A) 0.22 Ni per supercage; (B) 2.2 Ni per supercage.

orange species "$Ni(CO)_3$" has been reported from the reversible interaction of $Ni(CO)_4$ with NaX zeolite[10] or Al_2O_3.[5] However, IR studies alone cannot provide a definitive characterization of the metal coordination sphere.

We present here the first EXAFS spectra of $Ni(CO)_4$ adsorbed in different Y zeolites. Figure 4 compares both near edge spectra

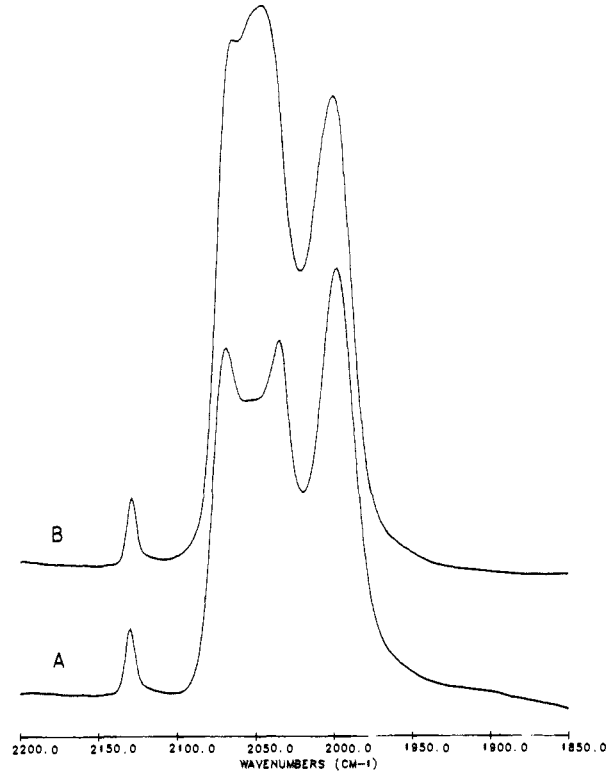

Figure 3. Infrared spectra of nickel tetracarbonyl in LiY zeolite: (A) 0.25 Ni per supercage; (B) 2.0 Ni per supercage.

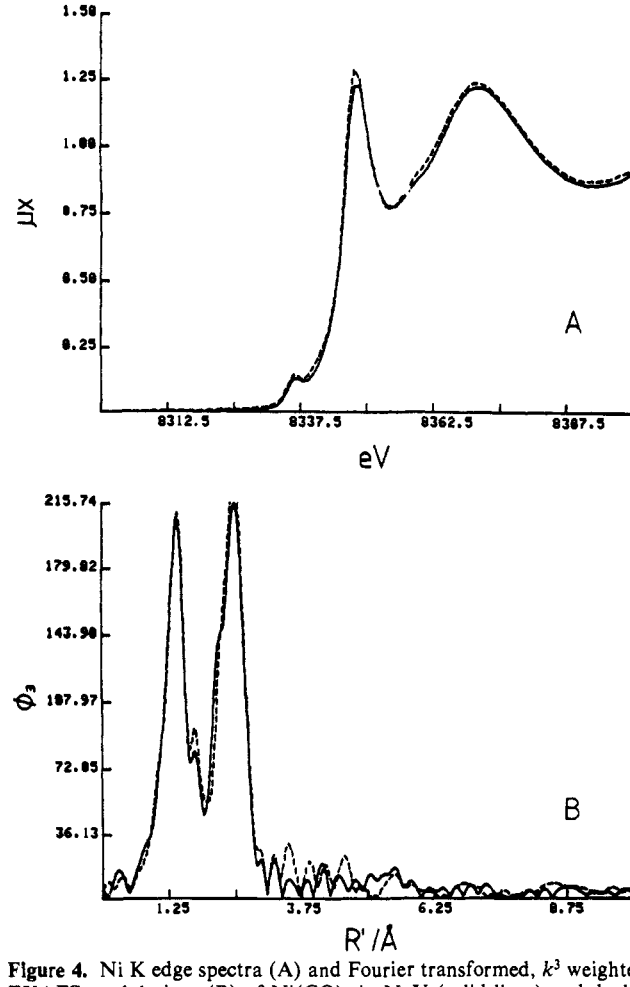

Figure 4. Ni K edge spectra (A) and Fourier transformed, k^3 weighted EXAFS modulations (B) of $Ni(CO)_4$ in NaY (solid lines) and dealuminated Y* (dashed lines). $R' = R + \beta(k)$, with $\beta(k)$ being the phase shift.

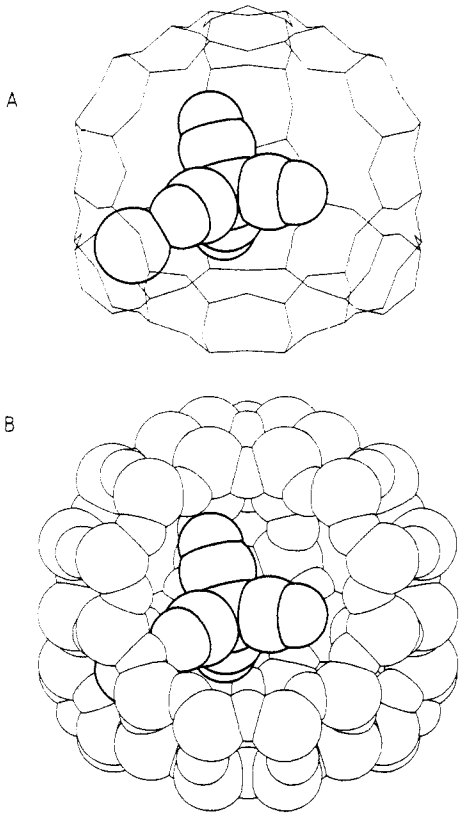

Figure 5. Model of $Ni(CO)_4$ binding to a Na^+ ion in the NaY supercage: (A) framework model; (B) model including zeolite van der Waals radii. Bond parameters for the cation–carbonyl bond and for bond angles were adopted from a crown ether–W–carbonyl adduct.[17]

and the Fourier transformed EXAFS modulations (Fts) of $Ni(CO)_4$ in dealuminated Y* and NaY. The complete match of both edge spectra and EXAFS Fts between the two samples indicates that adsorption of the carbonyl into the different forms of zeolite Y leads to essentially identical metal carbonyl species. No oxidation of the Ni is observed upon adsorption into the zeolite. Comparison of these edges with that of neat $Ni(CO)_4$ as well as comparison of the magnitude of the strong outer shell scattering due to linear CO indicates little distortion of the CO ligands. The two backtransformed peaks of both samples are similar to the data from the $Ni(CO)_4$ reference. These observations suggest that changes other than ligand displacement are responsible for the significant differences present in the IR spectra of these systems.

An explanation for the differences in the IR CO stretching pattern is the following: In dealuminated Y*, the $Ni(CO)_4$ is weakly adsorbed and undergoes moderate, isotropic perturbation of the symmetry which results in band broadening only. In contrast, the sodium cations in NaY represent an adsorption site with considerable Lewis acidity which interacts with one or more carbonyl ligands to form a Na^+--OC-Ni bridge. A similar interaction pattern has been discussed for the adsorption of metal carbonyls on alumina.[12] This carbonyl interaction may be comparable to the contact ion pairing of alkali metal cations with metal carbonyl anions.[13] The lowered symmetry of this complex makes the "totally symmetric" ν_1 mode infrared active as reported for solid $Ni(CO)_4$[14] and $Fe(CO)_5$ in alkali zeolites.[15] The T_d symmetry of $Ni(CO)_4$ has to be lowered to C_{2v} or less in order to account for the four observed bands.[16] A model of $Ni(CO)_4$ binding to a Na^+ ion in the NaY supercage is shown in Figure 5.

Table I. Bond Distances and Coordination Numbers of Ni Species in Zeolites As Derived from Fitting Fourier-Filtered EXAFS Data[a]

sample	distance/ Å	coordination no.	back-scatterer
Ni foil	2.492	12	Ni(0)
VAC323	2.47	5.3	Ni(0)
VAC373	2.46	6.2	Ni(0)
VAC673	2.48	7.6	Ni(0)
NiO	2.947	12	Ni(II)
OX295	2.94	6.8	Ni(II)
	2.43	0.9	Ni(0)
OX373	2.95	4.9	Ni(II)
	2.51	1.1	Ni(0)
OX673	similar to OX373		
$NaY(Ni(PMe_3)_x)_{0.5}$	+0.02[b]	3.96	P

[a] In addition to the above fitting parameters, the fits included allowances for changes in the Debye–Waller factor and in threshold energy. In all cases the changes of these parameters were small and chemically reasonable. [b] Since the Ni–P distance of this compound in solution is unknown, this fit provides the deviation from the reference data, estimated to be 2.30 Å.

The IR spectrum of $Ni(CO)_4$ in LiY is intermediate between Y* and NaY. At low Ni loadings, there are four carbonyl ligands due to cation-bound $Ni(CO)_4$. At higher loading, a single band for T_d $Ni(CO)_4$ is dominant. The concentration dependence of the spectrum can be explained by the cation occupations. In dehydrated NaY there are an average of 3.8 Na^+ ions per supercage in site II.[18] Even at high Ni loadings, every $Ni(CO)_4$ is bound to a sodium ion. However, in NaY that has been exchanged with Li^+ there are an average of 1.6 Na^+ and 0.9 Li^+ per supercage in site II.[19] Because there are fewer cations in the supercage of LiY, not every $Ni(CO)_4$ can bind to a cation at high Ni loadings.

2. Thermal Decomposition of $Ni(CO)_4$ in Y Zeolite. NaY loaded with 2.0 molecules of $Ni(CO)_4$ per supercage and heated up to 323 K in vacuo for 2 h (VAC323) loses weight corresponding to a coordinatively unsaturated system with CO/Ni = 1, accompanied by a color change from white to dark grey. No evidence has been found for loss of nickel metal since no metal mirror appeared. If NaY is *saturated* with 3.9/s.c., a similar decomposition experiment results in a metal mirror at the reactor wall.

The corresponding XANES of VAC323 is compared with the edge of $NaY(Ni(CO)_4)_2$ in Figure 6A. A dramatic reduction in the first absorption maximum indicates increased occupation of bonding orbitals upon removal of π-acceptor ligands as expected. The increase in pre-edge absorption can be understood in similar terms. These edge changes are indicative of the formation of metallic Ni, though some residual bound CO is still observed.

If the sample is evacuated at 373 K for 2 h (VAC373), further changes occur in the edge region (Figure 6B). Complete loss of CO is now observed as evidenced by comparison of the edges to that of Ni foil (Figure 6C). Continued heating to 673 K produces no further changes in the edge region. Gravimetric studies also show that all carbonyl ligands are desorbed at 373 K. The amount of loaded metal corresponds to the starting content and remains constant upon heating between 373 and 673 K.

The Fourier transform of sample VAC323 is compared to that of VAC373 in Figure 6D and allows for a similar interpretation as obtained from the K-edge results discussed above. After heating at 373 K no evidence for bound CO is observed and only minor differences in the particle size distribution occur.

The electron micrograph of VAC323 (Figure 7) shows octahedral Ni crystallites of 5–30-nm diameter, sticking at the *outer* surface of the zeolite matrix. Contributions of the 3rd and 4th Ni–Ni shell in the EXAFS Fts (Figure 6D) of this sample must

(12) Brown, T. L. *J. Mol. Catal.* **1981**, *12*, 41.
(13) Darensbourg, M. Y.; Barros, H. C. L. *Inorg. Chem.* **1979**, *18*, 3286.
(14) Jolly, P. W.; Wilke, G. *The Organic Chemistry of Nickel*; Academic: New York, 1974; Vol. 1, p 72ff.
(15) Bein, T.; Jacobs, P. A. *J. Chem. Soc., Faraday Trans. 1* **1983**, *79*, 1819; **1984**, *80*, 1391.
(16) Edgell, W. F.; Lyford, J., IV *J. Am. Chem. Soc.* **1971**, *93*, 6407.
(17) Cooper, M. K.; et al. *J. Chem. Soc., Dalton Trans.* **1981**, 2357.
(18) Breck, D. W. *Zeolite Molecular Sieves*; Reprint Edition; Krieger: Malabar, FL, 1984; p 100.
(19) Herden, H.; Einicke, W.-D.; Schollner, R.; Mortier, W.; Gellens, L. R.; Uytterhoeven, J. B. *Zeolites* **1982**, *2*, 131.

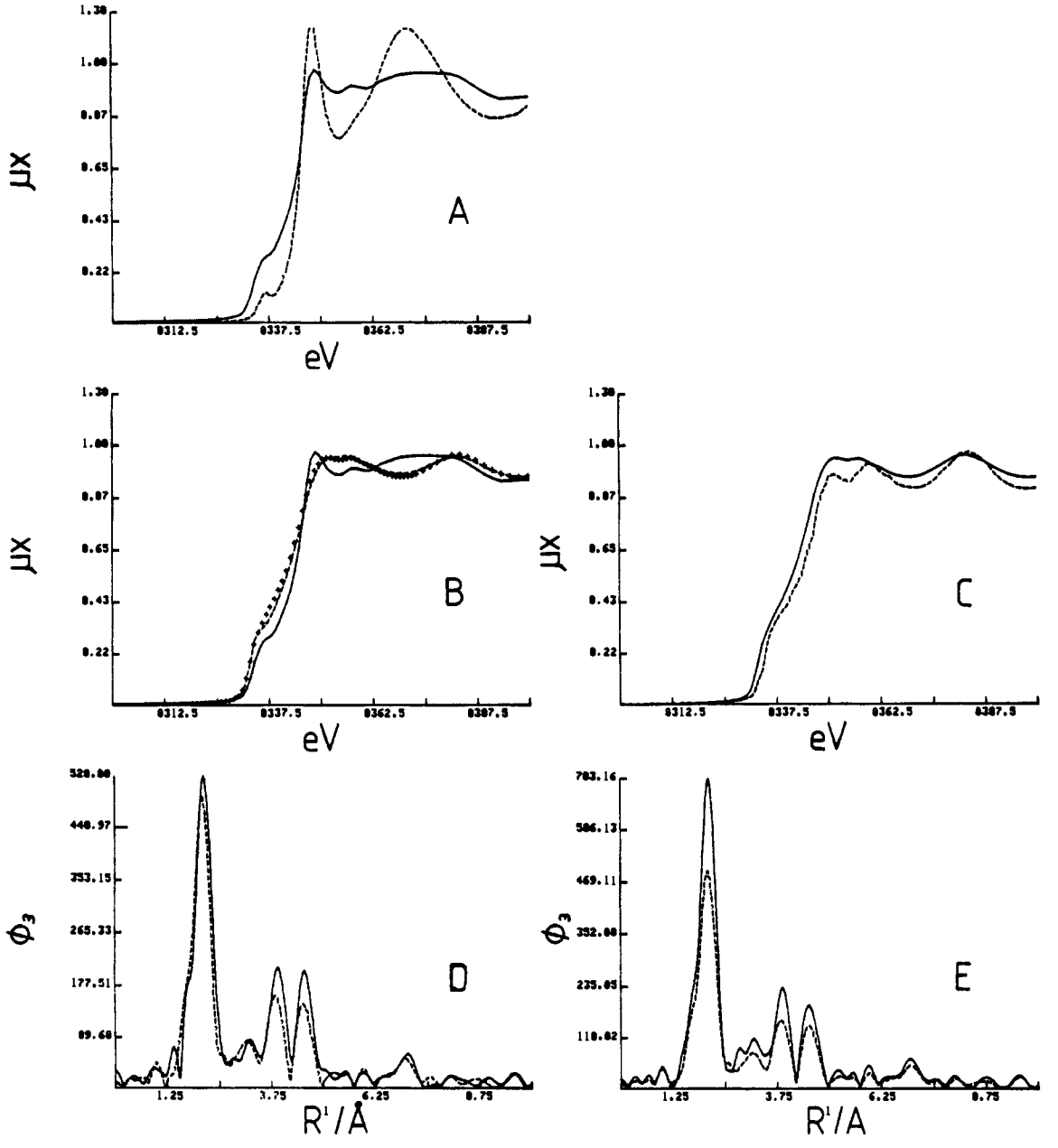

Figure 6. Ni K edge spectra (A, B, C) and Fourier transformed, k^3 weighted EXAFS modulations (Fts) of $Ni(CO)_4$ heat treated in NaY, $R' = R + \beta(k)$, with $\beta(k)$ being the phase shift. (A) Edges of $NaY\langle Ni(CO)_4)_2$ (dashed) and VAC323 (solid line). (B) Edges of samples VAC323 (—), VAC373 (--), and VAC673 (+). (C) Edges of sample VAC673 (—) and Ni foil (--). (D) Fts of samples VAC323 (—) and VAC373 (--). (E) Fts of samples VAC373 (--) and VAC673 (—).

be due to the larger particles that are detected in the TEM. Fitting of the backtransformed EXAFS modulations to Ni foil demonstrates that the first Ni–Ni scattering amplitude amounts to less than 50% of the bulk value (Table I). This value for the backscattering amplitude relates to an *average* particle size of 1.0 nm.[22] However, the bulk-like outer-shell Ni–Ni backscattering amplitude in the EXAFS data and the electron-optical observations indicate the presence of a fraction of larger Ni crystallites in this sample. On the basis of the first Ni–Ni amplitude, a maximum of 50% of the Ni atoms could be present as bulk-like particles (≥5 nm). For the remainder of the Ni phase, this extreme distribution would imply the complete absence of Ni–Ni neighbors, i.e., atomic dispersion with oxygen coordination by the zeolite framework. Since no appreciable oxygen coordination is detected in the Fts (in the expected Ni–O distance of approximately 0.20 nm), the authors favor a more realistic, bimodal size distribution with a major size fraction between ca. 0.5 and 1.5 nm (not detected in the electron microscope) and a fraction of large (5–30 nm) particles sticking at the outer surface of the zeolite crystals. It seems very likely that the small Ni particles have a size in the vicinity of the zeolite supercage dimensions (1.3 nm), since the rigid zeolite framework presents a barrier against agglomeration of the Ni phase.

Comparison of the later stages of thermal treatment (samples VAC373 and VAC673) in Figure 6E reveals a significant increase of Ni–Ni neighbor populations (Table I). This is indicative of an agglomeration process as expected for elevated temperatures.

EXAFS studies concerning the characterization of supported nickel metal particles have been reported.[20,21] Hydrogen reduction of $Ni^{II}/Si(OH)_4$ gels yielded Ni particles with diameters between 2 and 10 nm,[20] whereas larger particles were produced with a gas evaporation technique.[21] The magnitude of the EXAFS radial distribution function was found to decrease substantially with decreasing particle size.[21] It becomes clear that careful decom-

(20) Tohji, K.; Udagawa, Y.; Tanabe, S.; Ueno, A. *J. Am. Chem. Soc.* **1984**, *106*, 612.
(21) Hida, M.; Wada, N.; Maeda, H.; Terauchi, H.; Tsu, Y.; Kamijo, N. *Jpn. J. Appl. Phys.* **1985**, *24*, L3.
(22) Gregor, R. B.; Lytle, F. W. *J. Catal.* **1980**, *67*, 476.

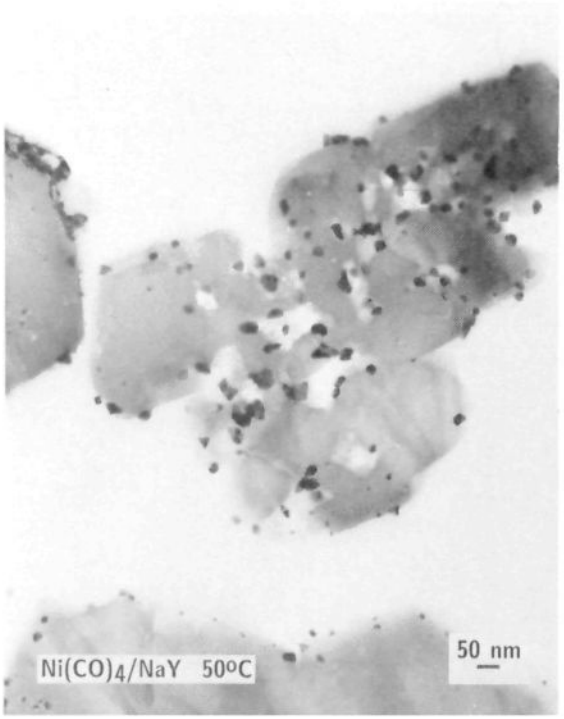

Figure 7. Electron micrograph of samples VAC323.

position of $Ni(CO)_4$ adsorbed in zeolites provides a valuable technique for the preparation of a significant fraction of small Ni particles.

3. Oxidation of Nickel Carbonyl in Faujasite. If the adduct $NaY\langle Ni(CO)_4\rangle_2$ (i.e., with 2 molecules per zeolite supercage) is exposed to an excess of molecular oxygen (relative to Ni) at 77 K and slowly warmed up to 295 K, the color of the sample changes from white to grey (OX295). Evacuation at 373 K reduces the weight down to the expected value for a complete oxidation to NiO (OX373). This weight remains unchanged upon further heating at 673 K for 12 h (OX673).

The Ni K edges of these samples are identical as shown in Figure 8A, indicating that the oxidation of $Ni(CO)_4$ in zeolite to Ni(II) species is extremely facile. The strong intensity of the first absorption maximum represents the "white line" of Ni(II). If the Fts of the respective EXAFS modulations are compared, only small differences are observed between the low temperature product OX295 and the samples treated at elevated temperatures (Figure 8B). Upon fitting to the backtransformed EXAFS modulations of the reference compounds, the first and the third marked peaks of the Ft from OX295 are assigned to Ni–O and Ni–Ni backscatters at distances typical for bulk NiO. A third peak, located between the former ones, is due to Ni–Ni distances in direct bonding, indicating that a small fraction of the Ni is still in the zerovalent state. The amplitude of the NiO contribution amounts to about 50% of the bulk value, which translates into a particle size distribution around 1 nm,[22] provided the distribution is monomodal and the degree of disorder is comparable to bulk NiO (Table I). An inspection of the corresponding electron micrograph (Figure 9) shows that only very few NiO crystallites are located outside the zeolite interior, thus the major fraction of the Ni must be stabilized within the zeolite cage system. This is in marked contrast to the significant migration of metal which is observed upon *thermal* decomposition of the carbonyl/zeolite adduct. It is evident that the NiO/NaY system is remarkably stable against sintering since neither the degree of oxidation nor the average particle size change upon heating up to 673 K (Table I).

4. Adsorption of Ni–Carbonyl–Phosphine Complexes in Y Zeolite. Both $Ni(CO)_2(PMe_3)_2$ and $Ni(CO)_3PMe_3$ are readily adsorbed from hexane by NaY. A space-filling model of $Ni(CO)_3PMe_3$ in the NaY supercage shows that the Ni complex

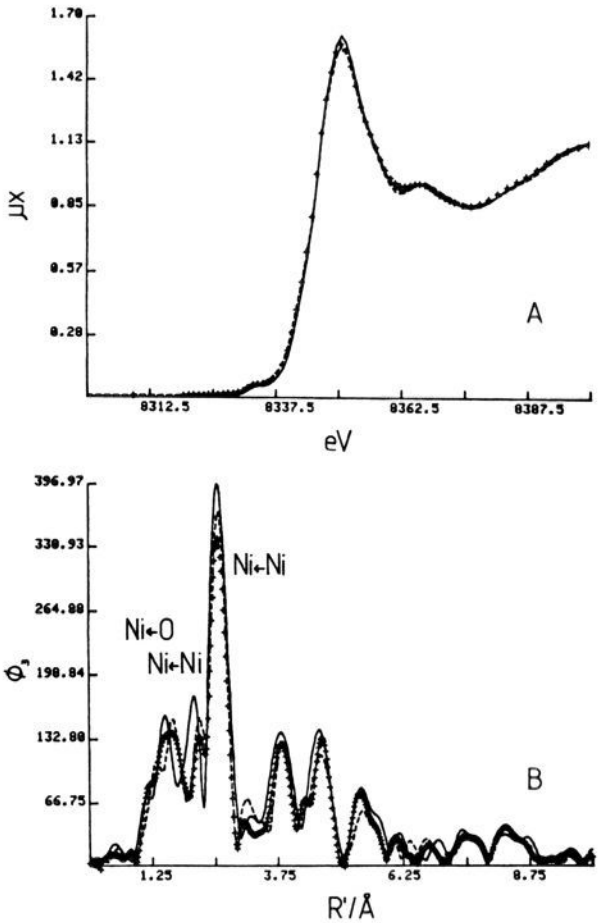

Figure 8. Ni K edge spectra (A) and Fourier transformed, k^3 weighted EXAFS modulations (B) of $Ni(CO)_4$ oxidized in NaY, $R' = R + \beta(k)$, with $\beta(k)$ being the phase shift. Sample OX295 (—), OX373 (--), and OX673 (+).

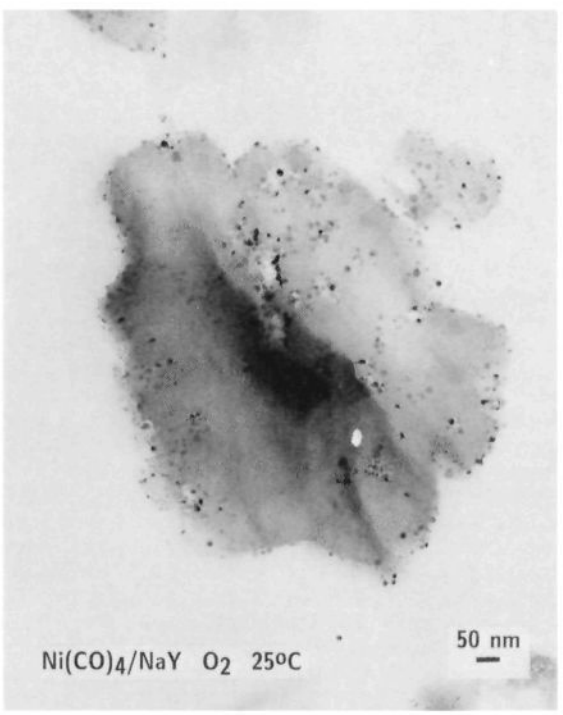

Figure 9. Electron micrograph of sample OX295.

should be able to pass through the 12-ring opening into the supercage (Figure 10). The saturation loading levels are 1.48 Ni

Table II. Spectroscopic Data for Ni–Phosphine Complexes in NaY

sample	ν(CO)/cm^{-1}	^{31}P NMR/ppm: complex (A)	^{31}P NMR/ppm: free ligand (B)[a]	ligand shift, A–B
I				
$NaY\langle Ni(CO)_3P(t\text{-}Bu)_3\rangle_{0.5}$	2046, 1942 2067, 1972	+91.1	+62.5	28.6
$Ni(CO)_3P(t\text{-}Bu)_3$	2061, 1984			
$Ni(CO)_3P(t\text{-}Bu)_3$[b]	2060, 1980	+90.9	+62.5	28.4
II				
$NaY\langle Ni(CO)_3PMe_3\rangle_{1.48}$	2059, 1975	−19.3	(−59.7)	40.4
$NaY\langle Ni(CO)_3PMe_3\rangle_{0.25}$	2065, 1992, 1958	−18.5	−53.3	40.8
$Ni(CO)_3PMe_3$	2070, 1996	−19.8	−61	41.2
$Ni(CO)_3PMe_3$[c]	2069, 1994	−19.9[g]	−61[g]	41.1
III				
$NaY\langle Ni(CO)_2(PMe_3)_2\rangle_{0.97}$	1965 (sh), 1954 1899, 1880	−17.4	(−59.7)	42.3
$Ni(CO)_2(PMe_3)_2$	2002, 1943	−17.5	−61	43.5
$Ni(CO)_2(PMe_3)_2$[d]	2002, 1941	−18.2[g]	−61	42.8
IV				
$NaY\langle Ni(CO)_3PPh_2(CHMe_2)\rangle_{0.25}$	2075, 1995, 1948	40.5	5.8	34.7
$Ni(CO)_3PPh_2(CHMe_2)$	2067, 1990 (CH_3CN)			
V				
$NaY\langle Ni(PMe_3)_x\rangle_{0.5}$	–	−19.3	−59.7	40.4
$Ni(PMe_3)_4$	–	−21.2	−61	39.8
$Ni(PMe_3)_4$[f]	–	−22.2	−63.3	41.1

[a] For zeolite samples, this value is the chemical shift of the uncomplexed phosphine adsorbed into the zeolite. [b] Schumann, H.; Rosch, L.; Neumann, H.; Kroth, H.-J. *Chem. Ber.* **1975**, *108*, 1630. [c,d] Bigorgne, M. *J. Inorg. Nucl. Chem.* **1964**, *26*, 107. [e] Chatt, J.; Hart, F. A. *J. Chem. Soc., London* **1960**, 1378. [f] Tolman, C. A.; Seidel, W. C.; Gosser, L. W. *J. Am. Chem. Soc.* **1974**, *96*, 53. [g] Mathieu, R.; Lenzi, M.; Poilblanc, R. *C.R. Acad. Sci., Ser. C* **1968**, *266*, 806. [h] Grim, S. O.; Briggs, W. L.; Barth, R. C.; Tolman, C. A.; Jesson, J. P. *Inorg. Chem.* **1974**, *13*, 1095.

per supercage for $Ni(CO)_3PMe_3$ and 0.97 Ni per supercage for $Ni(CO)_2(PMe_3)_2$.

IR spectra and ^{31}P NMR spectra are summarized in Table II. The ^{31}P NMR shift remains largely unaffected when a complex is introduced into the zeolite. This makes ^{31}P NMR a valuable tool for the identification of compounds adsorbed or synthesized in zeolites. In favorable cases with narrow line widths, chemical shift differences as small as 2–3 ppm can be resolved by solid-state MAS–NMR. In contrast to the NMR results, the infrared spectra of the Ni complexes change dramatically when they are introduced into the zeolite. With $Ni(CO)_3L$ and $Ni(CO)_2L_2$ having C_{3v} and C_{2v} symmetry, respectively, two CO stretching vibrations are expected in each case (A_1, E and A_1, B_1).[14] It is known that interaction with polar solvents decreases the energy of both modes. The low-frequency mode (E) is more strongly affected than the high-frequency mode in $Ni(CO)_3L$.[14] The IR data in Table II show decreases in the carbonyl stretching frequency of up to 63 cm^{-1} when complexes are adsorbed by NaY. The zeolite could therefore be regarded as an extremely polar solvent for the metal complex. Once this effect is appreciated, the IR spectrum is useful for the assignment of the structure. For example, a carbonyl band at >2000 cm^{-1} is a clear indication of a $Ni(CO)_3L$ species.

5. Synthesis of Ni–Phosphine Complexes within Y Zeolite. An alternative way to make $NaY\langle Ni(CO)_3L\rangle$ is by synthesis of the Ni complex inside the zeolite supercage. For example, $Ni(CO)_3PMe_3$ can be synthesized in NaY by solution loading of PMe_3 from hexane (0.25 equiv per supercage) followed by vapor-phase loading of excess $Ni(CO)_4$. IR spectroscopy shows that the product zeolite contains excess $Ni(CO)_4$. Most of the $Ni(CO)_4$ and part of the $Ni(CO)_3PMe_3$ can be displaced from the zeolite by a single THF wash. The displacement of these Ni complexes by THF is expected since they are both small enough to pass through the 12-ring opening of the supercage (Figures 5 and 10). The IR spectrum of the THF-washed sample is significantly different from $NaY\langle Ni(CO)_3PMe_3\rangle_{1.48}$ prepared by solution loading of the preformed Ni complex (Table II). The differences may be due to loading effects or solvent effects. This illustrates the difficulty of using IR spectroscopy as the sole method of characterization. Unlike EXAFS or ^{31}P spectroscopy, IR spectroscopy is very sensitive to the environment around the metal complex.

$Ni(CO)_3(PPh_2CHMe_2)$ was synthesized within the supercage of NaY by solution loading of PPh_2CHMe_2, followed by vapor-phase loading of excess $Ni(CO)_4$. ^{31}P MAS–NMR spectroscopy shows the complete conversion of the phosphine in the zeolite (Figure 11B) to zeolite entrapped $Ni(CO)_3(PPh_2CHMe_2)$ (Figure 11A). The sidebands in Figure 11A are due to the incomplete averaging of the chemical shift anisotropy by the magic angle spinning. When this sample was washed with THF, only the $Ni(CO)_4$ was displaced from the zeolite. The $Ni(CO)_3(PPh_2CHMe_2)$ is too large to fit through the 12-ring opening of the supercage (Figure 12). This material is comparable to a ship

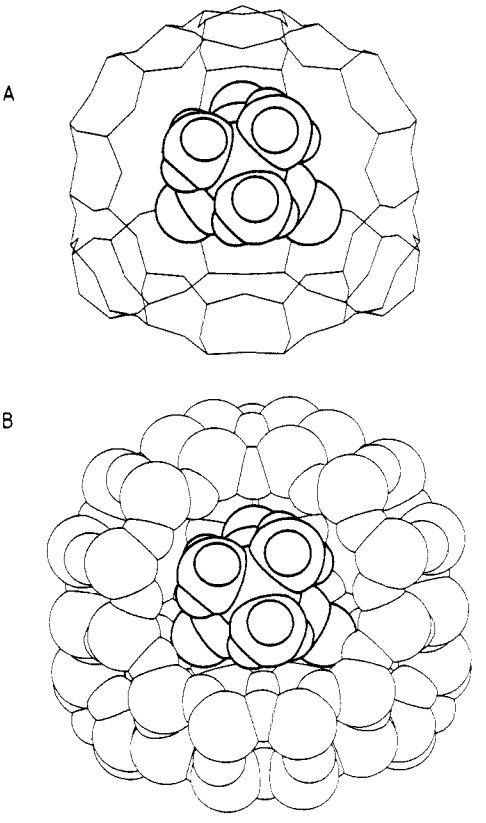

Figure 10. Model of $Ni(CO)_3PMe_3$ in the NaY supercage: (A) framework model; (B) model including zeolite van der Waals radii.

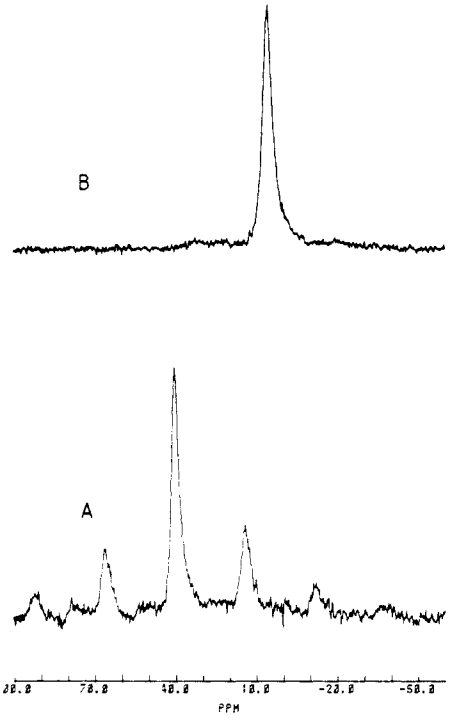

Figure 11. ^{31}P MAS-NMR spectra of (A) NaY⟨Ni(CO)$_3$(Ph$_2$PCHMe$_2$)⟩ and (B) NaY(Ph$_2$PCHMe$_2$⟩.

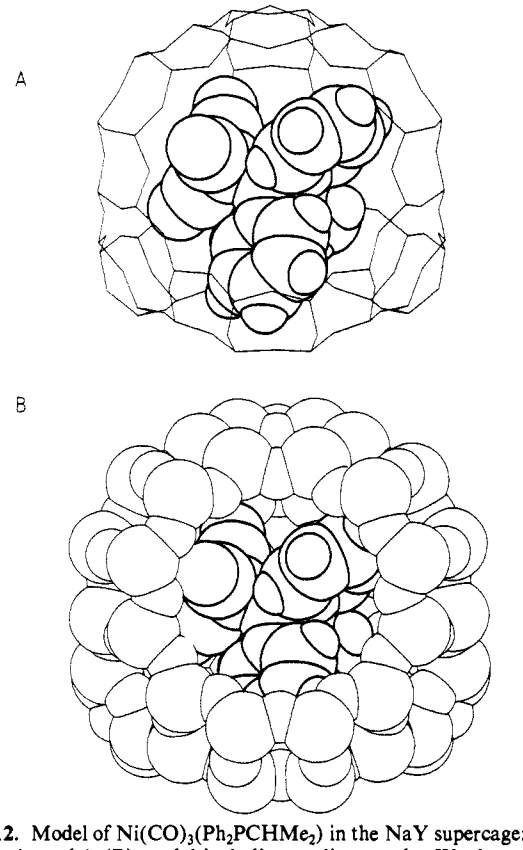

Figure 12. Model of Ni(CO)$_3$(Ph$_2$PCHMe$_2$) in the NaY supercage: (A) framework model; (B) model including zeolite van der Waals radii.

in the bottle; the reactants are small enough to enter the zeolite supercage but the product is too large to exit.

A modification of the above procedure was used to prepare zeolite entrapped Ni(CO)$_3$P(t-Bu)$_3$. P(t-Bu)$_3$ and Ni(CO)$_4$ were added to the zeolite sequentially from hexane solution. The ^{31}P MAS-NMR spectrum of the zeolite product has a resonance at 91.1 ppm equal to the chemical shift of Ni(CO)$_3$P(t-Bu)$_3$ in solution and a resonance at 62.5 ppm that is assigned to unreacted

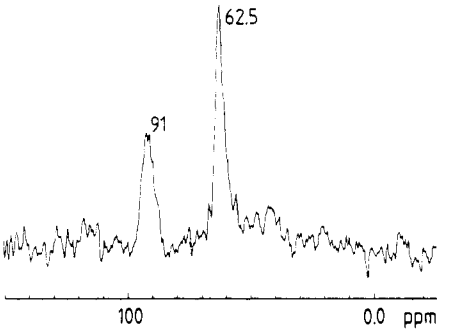

Figure 13. ^{31}P MAS-NMR spectrum of NaY⟨Ni(CO)$_3$P(t-Bu)$_3$⟩$_{0.5}$.

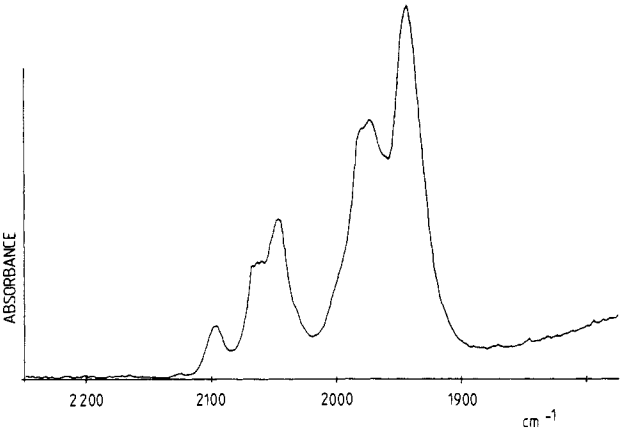

Figure 14. Infrared spectrum of the CO stretching region of sample NaY⟨Ni(CO)$_3$P(t-Bu)$_3$⟩$_{0.5}$.

phosphine in the zeolite (Table II, Figure 13). It should be noted that unreacted phosphine cannot be detected by either IR or Ni EXAFS. The IR spectrum of NaY⟨Ni(CO)$_3$P(t-Bu)$_3$⟩$_{0.5}$ has at least five bands in the carbonyl region Figure 14). The complexity of the spectrum may be due to a mixture of cation-bound species (Na^+--OC-Ni) and cation-free species as was observed with Ni(CO)$_4$ in LiY. There may also be a splitting of the E mode in the cation-bound species. Splitting of the E mode is sometimes seen even in solution spectra of Ni(CO)$_3$L complexes.[14]

The Ni K edge and the Fts of NaY⟨Ni(CO)$_3$P(t-Bu)$_3$⟩$_{0.5}$ are compared to those of authentic Ni(CO)$_3$P(t-Bu)$_3$ in Figure 15. The edges match perfectly, indicating that a similar electron density is present at the Ni central atoms of both species. If the radial distribution functions are compared, a close match is observed for the magnitudes of the first (Ni–C) and third (Ni–C–O) peak (Figure 15B). The differences present in the second peak (Ni–P) are assigned to small artifacts caused by the convolution of three strong backscattering patterns; it is known that side lobes of strong shell contributions add in the Fts if the shells are close in R space. Individual peaks could not be filtered out to yield neighbor distances and coordination numbers due to lack of sufficient resolution. However, the backtransformed region of the three backscatterers compared well with that of the reference.

The sequential addition of Ni(allyl)$_2$ and excess PMe$_3$ to NaY from pentane solution yields zeolite-entrapped Ni(PMe$_3$)$_x$. The ^{31}P MAS-NMR spectrum of this sample shows a peak for unreacted PMe$_3$ and a peak close to the position expected for Ni(PMe$_3$)$_4$ (Table II). A space-filling model shows that there is enough space to accommodate the Ni complex inside the NaY supercage without any van der Waals contacts (Figure 16).

The Ni K edge of an authentic solution sample of Ni(PMe$_3$)$_4$ is compared to the zeolite adduct in Figure 17a. As with the samples discussed previously, there is a good match between the edges of reference and zeolite adduct sample. The phosphine ligands decrease the electron density on the Ni atom as dramatically visualized in the overlay of the Ni(CO)$_4$ edge and the Ni(PMe$_3$)$_4$ edge (Figure 17B). The first absorption maximum in the carbonyl edge vanishes and a weak maximum at lower

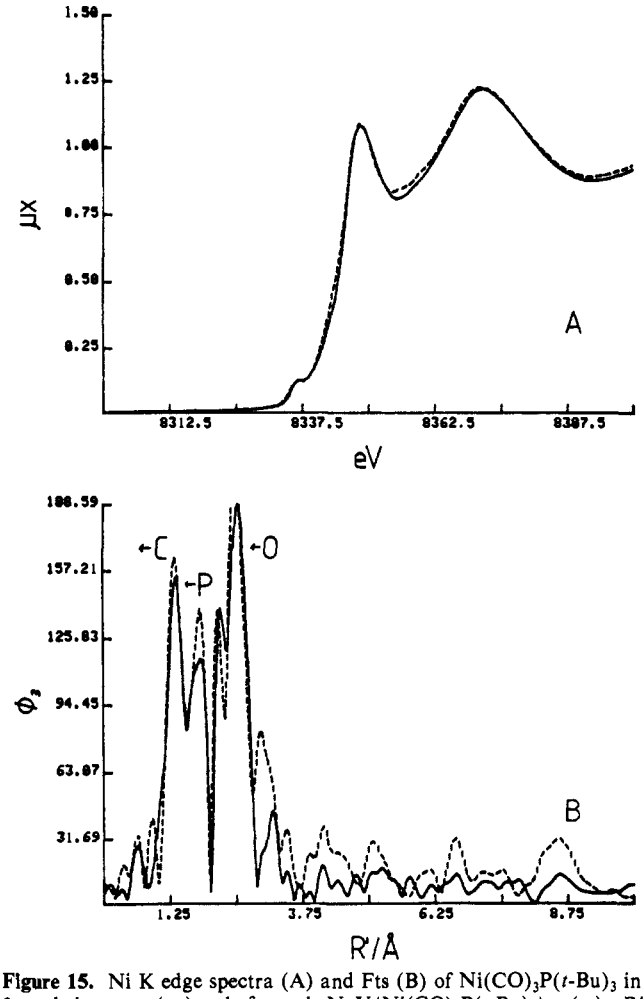

Figure 15. Ni K edge spectra (A) and Fts (B) of $Ni(CO)_3P(t\text{-}Bu)_3$ in 3-methylpentane (—) and of sample $NaY(Ni(CO)_3P(t\text{-}Bu)_3)_{0.5}$ (--). $R' = R + \beta(k)$, with $\beta(k)$ being the phase shift.

energy is observed. The EXAFS radial distribution function of the zeolite adduct shows a first shell contribution matching with that of the $Ni(PMe_3)_4$ reference system (Figure 17C). However, a significant decrease in amplitude is observed for the zeolite adduct. Since the Ni–C distance in $Ni(allyl)_2$ is close to the Ni–P bond distance (0.21–0.22 nm), it cannot be ruled out that the reaction was incomplete. Owing to the high reactivity of $Ni(allyl)_2$ and the excess of PMe_3, this explanation seems unlikely. Tris-phosphine nickel complexes have been prepared in solution.[23] On the basis of the UV spectrum of $Ni(PEt_3)_3$ (λ_{max} = 500 nm), we would expect $Ni(PMe_3)_3$ to be purple, whereas our zeolite sample is pale yellow. Further analysis of the backtransformed back-scatterer region (Table I) demonstrates that the decrease in amplitude is not due to a decrease in coordination number but is a result of static disorder. A tentative explanation for this disorder effect would be elongation of one of the Ni–P bonds as a result of its orientation in the zeolite supercage. Molecular modeling shows that $Ni(PMe_3)_4$ can fit inside the zeolite supercage (Figure 16). The figure demonstrates how crowded the cage becomes upon accommodation of the Ni complex.

Summary

The combined use of EXAFS, X-ray near edge spectroscopy, MAS–NMR, and IR yields consistent information about the oxidation state, agglomeration processes, and intrazeolite chemistry of organonickel compounds adsorbed in the cage system of Y zeolites.

Upon adsorption, $Ni(CO)_4$ undergoes symmetry changes due to CO cation bonding. Small nickel–phosphine complexes can be adsorbed from hydrocarbon solution. Alternatively, nickel–phosphine complexes can be synthesized inside the zeolite supercage by sequential addition of the phosphine and the Ni reagent. In the case of bulky phosphines, this gives nickel–phosphine complexes that are too large to exit the zeolite.

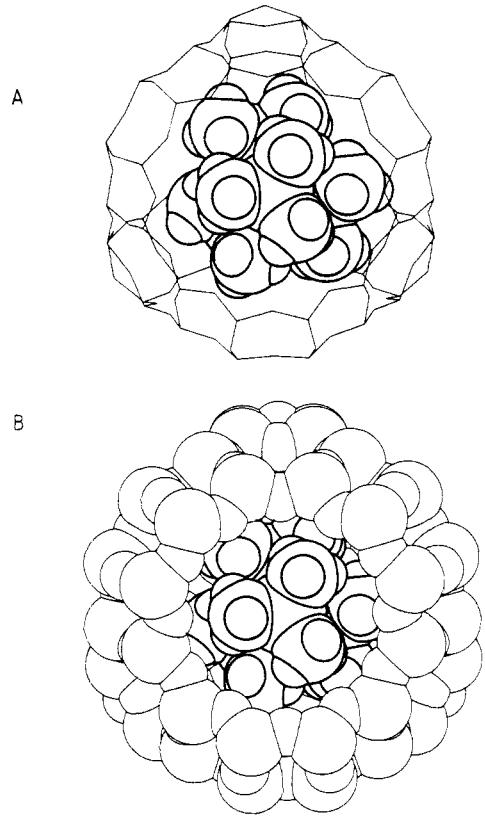

Figure 16. Model of $Ni(PMe_3)_4$ in the NaY supercage: (A) framework model; (B) model including zeolite van der Waals radii.

Experimental Section

All operations involving dehydrated zeolites, $Ni(CO)_4$, and phosphines were done either in a Vacuum Atmospheres glovebox under nitrogen or on a high-vacuum line.

Materials. Zeolite NaY from Strem Chemicals (Linde LZ-Y52), with the unit cell composition $Na_{55}(AlO_2)_{55}(SiO_2)_{137}\cdot xH_2O$, was dehydrated at 670 K under 10^{-5} Torr for 12 h (heating rate 2 deg K/min) and handled under nitrogen in a drybox ($p(H_2O) < 0.5$ ppm). LiY was prepared by exchanging 10 g of NaY zeolite three times with 300 mL of 10% $LiNO_3$ solution for 60 min at 360 K. The zeolite was dehydrated by heating to 870 K (1 deg K/min) at $\leq 10^{-5}$ Torr and maintaining at 870 K for 8 h. Dealuminated zeolite Y* was prepared essentially according to Grobet et al.[24] using a vertically mounted tube furnace for the $SiCl_4$ and steam treatments. Analysis gave a unit cell composition of $Na_{0.04}Al_{0.44}Si_{191.6}O_{384}$.

$Ni(CO)_4$ from Alfa and PMe_3 and $P(t\text{-}Bu)_3$ from Strem were used as received. THF was distilled from sodium benzophenone ketyl under argon. All other solvents were sparged with argon, passed through activity I alumina in the drybox, and stored over activated 4A molecular sieve until use. $Ni(allyl)_2$ was prepared as a pentane solution by a literature procedure.[25] The Ni concentration was determined by treating an aliquot with dry oxygen to give a dark precipitate which was analyzed for Ni.

Sample Preparation. Vapor-Phase Loading with $Ni(CO)_4$. Half a gram of dehydrated zeolite were weighted into a quartz sample holder in the drybox, introduced into a vertical quartz reactor, and evacuated at 10^{-5} Torr for 30 min. $Ni(CO)_4$ was degassed at the same vacuum line by carrying out 3 freeze–pump–thaw cycles under low-intensity light. A calculated amount of $Ni(CO)_4$ vapor was admitted to the zeolite and allowed to equilibrate for 30 min at 295 K, followed by evacuation for 30 min. The evacuation step was omitted for some samples. This was especially important for samples of dealuminated Y since evacuation resulted in partial loss of the $Ni(CO)_4$. The weight gain of the zeolites

(23) Tolman, C. A.; Seidel, W. C.; Gosser, L. W. *J. Am. Chem. Soc.* **1974**, *96*, 53.

(24) Grobet, P. J.; Jacobs, P. A.; Beyer, H. K. *Zeolites* **1986**, *6*, 47.

(25) O'Brien, S.; Fishwick, M.; McDermott, B.; Wallbridge, M. J. H.; Wright, J. A. *Inorg. Synth.* **1971**, *13*, 73.

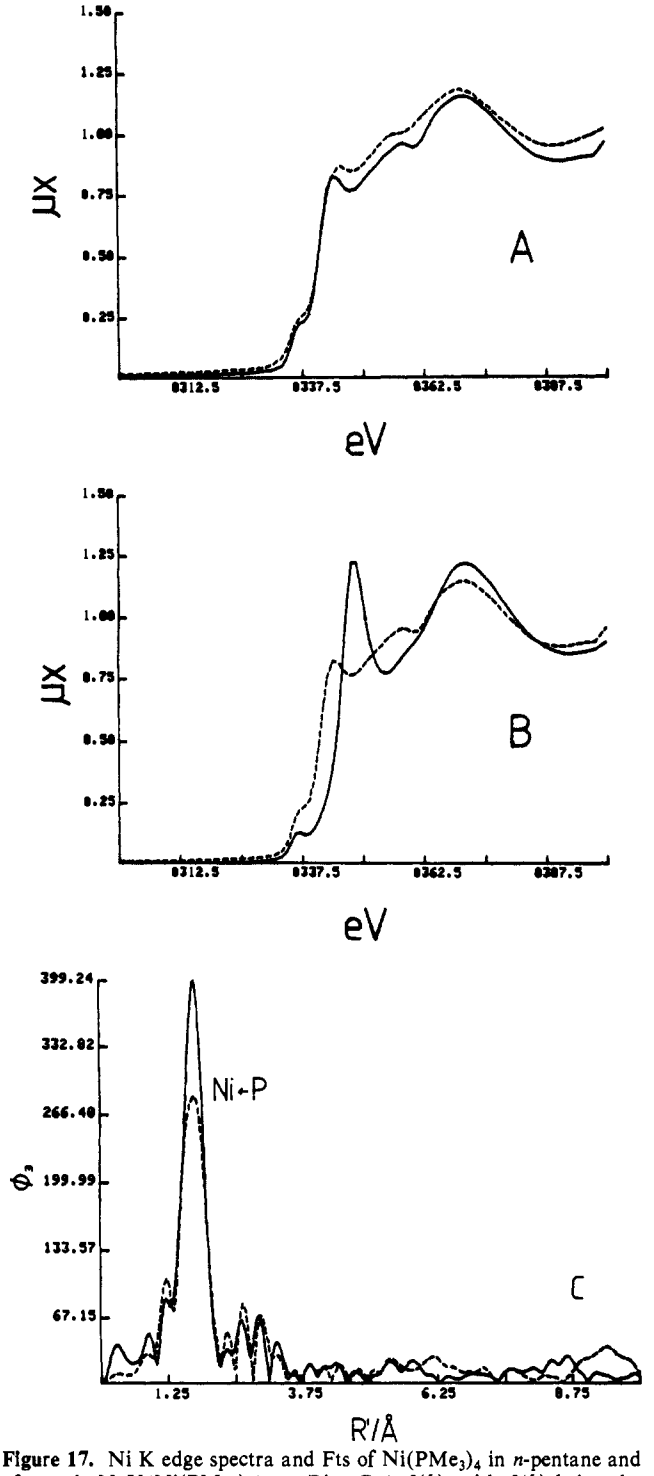

Figure 17. Ni K edge spectra and Fts of $Ni(PMe_3)_4$ in *n*-pentane and of sample $NaY\langle Ni(PMe_3)_x\rangle_{0.5}$. $R' = R + \beta(k)$, with $\beta(k)$ being the phase shift. (A) Edges of the reference (—) and of sample $NaY\langle Ni(PMe_3)_x\rangle_{0.5}$ (--); (B) edges of $Ni(PMe_3)_4$ in *n*-pentane (--) and of sample $NaY\langle Ni(CO)_4\rangle_2$ (—); and (C) Fts of $Ni(PMe_3)_4$ in *n*-pentane (—) and of $NaY\langle Ni(PMe_3)_x\rangle_{0.5}$ (--).

was used to confirm the accuracy of the manometric dosing procedure. For saturation loadings, the evacuated zeolites were exposed for 60 min to the full vapor pressure from a container of liquid $Ni(CO)_4$ held at 273 K.

Thermal Decomposition of $NaY\langle Ni(CO)_4\rangle$. Samples of ca. 300 mg were heated under vacuum, with a rate of 1 deg K/min, up to 323, 373, and 673 K (samples VAC323, VAC373, and VAC673), and held at these temperatures for 2 and 12 h (at 673 K). Weight changes were monitored after each heating cycle and the respective samples were stored under nitrogen.

Synthesis of $NaY\langle Ni(CO)_3PMe_3\rangle_{1.48}$ (i.e., with an average loading of 1.48 molecules per supercage). A solution of $Ni(CO)_3PMe_3$ was prepared by combining $Ni(CO)_4$ (0.683g, 4.0 mmol) and PMe_3 (0.304g, 4.0 mmol) in 50 mL of hexane. After 2 h, dehydrated NaY zeolite (1.595 g, 1.00 mmol supercages) was added while stirring. The solution concentration of $Ni(CO)_3PMe_3$ was monitored by IR spectroscopy of filtered aliquots. After 20 h, the solution concentration was no longer changing. The saturation loading of the zeolite was calculated as 1.48 Ni per supercage. The zeolite was filtered and dried briefly on the frit.

Synthesis of $NaY\langle Ni(CO)_2(PMe_3)_2\rangle_{0.97}$. $Ni(CO)_4$ (18.8 mL, 0.10 M) and PMe_3 (20.1 mL, 0.20 M) were combined in a 200-mL flask. The solution was frozen and the flask was evacuated and closed off with a high-vacuum Teflon stopcock. The solution was heated to 348 K for 2 h. An IR spectrum showed complete conversion to $Ni(CO)_2(PMe_3)_2$. Dry NaY zeolite (1.179 g, 0.627 mmol) was added with stirring, and after 48 h a saturation loading of 0.97 Ni per supercage was obtained. The zeolite was filtered and dried briefly on the frit.

Synthesis of $NaY\langle Ni(CO)_3PPh_2(CHMe_2)\rangle_{0.25}$ and $NaY\langle Ni(CO)_3PMe_3\rangle_{0.25}$. Dry NaY (0.833 g, 0.522 mmol of supercages) was stirred in 25 mL of hexane for 15 min. A solution of $PPh_2(CHMe_2)$ (0.030 g, 0.131 mmol) in 5 mL of hexane was added dropwise over a period of 5 min. The UV spectrum of a filtered aliquot showed that all of the phosphine had been adsorbed after 20 min. The zeolite was filtered and dried at $<10^{-5}$ Torr for 2 h. The evacuated zeolite was exposed for 60 min to the full vapor pressure from a container of liquid $Ni(CO)_4$ held at 273 K. ^{31}P MAS-NMR spectroscopy showed complete reaction of the $PPh_2(CHMe_2)$, and IR spectroscopy showed an excess of $Ni(CO)_4$ in the zeolite. A small sample (ca. 0.050 g) was stirred in 2.0 mL of THF for 2 h. The filtered zeolite showed IR bands only for entrapped $Ni(CO)_3PPh_2(CHMe_2)$ (Table II). A similar procedure was used to prepare $NaY\langle Ni(CO)_3PMe_3\rangle_{0.25}$ except that the THF washing causes a partial loss of $Ni(CO)_3PMe_3$ so that the Ni loading in the sample characterized by IR (Table II) was <0.25 Ni per supercage.

Synthesis of $NaY\langle Ni(CO)_3P(t\text{-}Bu)_3\rangle_{0.5}$. Dry zeolite (1.000 g, 0.626 mmol supercages) was suspended in 25 mL of hexane and stirred for 10 min. A solution of $P(t\text{-}Bu)_3$ (63 mg, 0.311 mmol) in 25 mL of hexane was added dropwise to the zeolite suspension while stirring. The mixture was stirred for 12 h at 295 K. Under stirring, a solution of $Ni(CO)_4$ (0.10 M in hexane, 6.3 mL, 100% excess) was added dropwise and the suspension was stirred for 12 h. The zeolite was filtered and dried briefly on the frit.

Synthesis of $NaY\langle Ni(PMe_3)_4\rangle_{0.5}$. Dry zeolite (1.00 g) was suspended in 25 mL of pentane and stirred for 30 min. The $Ni(allyl)_2$ solution (2.96 mL, 0.106 M) was added dropwise to the zeolite suspension while stirring. The mixture was stirred for 45 min during which time the yellow solution decolorized and the zeolite became orange. A solution of PMe_3 (12.6 mL, 0.20 M, 100% excess) was added dropwise over a period of ca. 2 min and the suspension was stirred for 12 h. The pale yellow zeolite was filtered and dried briefly on the frit.

Reference solutions of all Ni compounds were prepared for the EXAFS studies.

Analytical Methods. IR Spectroscopy. IR spectra were taken with a Nicolet 5DXB FT-IR spectrometer, in sample holders equipped with CaF_2 windows. It was found that $Ni(CO)_4$ was displaced from the zeolite by THF, hexane, or Nujol hydrocarbons. Therefore, IR spectra of $Ni(CO)_4$-zeolite samples were recorded as thin dry powders between CaF_2 plates. The edges of the plates were sealed with high-vacuum grease to exclude air. Zeolite-Ni-phosphine samples could be examined in Nujol mull. Solution spectra were recorded in pentane or hexane. Typically 200 scans were accumulated with a resolution of 2 cm^{-1}.

EXAFS Studies. The EXAFS experiments were carried out at the X-11A beamline at the National Synchroton Light Source with a stored electron energy of 2.5 GeV at currents between 35 and 100 mA. Spectra were taken of (i) thermostable compounds embedded at 310 K in dodecane/octadecane (1:1), (ii) $Ni(CO)_4$/zeolite adducts in 1-mm sealed polyethylene cells, and (iii) reference solutions in 1-mm sealed polyethylene cells, in a Dewar with Kapton windows at ca. 100 K. In most cases, IR spectra were recorded after the EXAFS experiment to confirm the stability of the samples. The data were analyzed according to published procedures.[26] Background removal was accomplished by using a cubic spline function and the resultant EXAFS modulations were weighted by k^3 and Fourier transformed over a range of 2 to 16 k. Typically, the EXAFS data of the zeolite-encapsulated Ni complexes were directly compared with the respective reference compounds. Additionally, individual coordination shells were examined by comparison of the backtransformed EXAFS modulations of the samples to well-defined reference compounds (Ni foil, NiO, $Ni(CO)_4$, etc.). Coordination numbers and bond distances were obtained from an iterative fitting routine using experimentally determined phase and amplitude functions from both reference and unknown. Variable fitting parameters included

(26) Lee, P. A.; Citrin, P. A.; Eisenberger, P. M.; Kincaid, B. M. *Rev. Mod. Phys.* **1981**, *53*, 769.

bond distance, coordination number, Debye-Waller factor (Δs^2), and threshold energy (ΔE_0). The EXAFS radial distribution functions obtained by Fourier transformation have not been corrected for phase shifts (β), and therefore show deviations from actual neighbor distances R in real space by 0.02 to 0.05 nm. The apparent distances $R' = R + \beta$ are indicated in the corresponding figures.

The ^{31}P **MAS-NMR spectra** were obtained on a Bruker CXP-300 instrument. Andrews type rotors were filled with ca. 200 mg of sample in the drybox and introduced into the NMR probe in a glovebag under flowing nitrogen. Dry nitrogen was used as a drive gas for the rotor to obtain spinning rates between 2 and 4 kHz. A 30° to 90° pulse with 10-s recycle time was used, depending on the T_1, to obtain quantitative spectra. H-decoupling time was 20–60 ms. Chemical shifts were referred to 85% H_3PO_4. No significant oxidation of the samples was observed during the NMR experiments. The solution $^{31}P\{^1H\}$ NMR spectra were recorded in mixtures of pentane or hexane with C_6D_6.

Electron Micrographs were taken on an Hitachi H600 from microtomed sections of 80–90-nm thickness. Samples were embedded in EPON 812 under exclusion of air.

Molecular modeling was done with Chem-X software developed and distributed by Chemical Design Ltd., Oxford, England, on a VAX 8650 computer. Bond lengths and angles from known crystal structures were used wherever possible. Unknown structure parameters were estimated from known structures. Most structures had their van der Waals energy minimized by an iterative process which allowed rotation about single bonds and translation and rotation of the guest molecule within the fixed zeolite supercage.

Acknowledgment. The authors acknowledge the following people: Dr. Steve Heald, Larry Fereria, and Jack Scrofani of Brookhaven National Laboratory assisted in data collection. Mike Van Kavelaar of DuPont prepared the electron micrographs, and David Rothfuss of DuPont provided general technical assistance. K.M. is grateful for a grant from Deutsche Forschungsgemeinschaft. The operational funds for NSLS beamline X11A are supported by DOE Grant DE-AS05 80ER10742.

Registry No. $Ni(CO)_3P(t\text{-}Bu)_3$, 22955-41-5; $Ni(CO)_3PMe_3$, 16406-99-8; $Ni(CO)_2(PMe_3)_2$, 16787-34-1; $Ni(CO)_3PPh_2(CHMe_2)$, 112320-39-5; $Ni(CO)_4$, 13463-39-3; $Ni(allyl)_2$, 12077-85-9; NiO, 1313-99-1; Ni, 7440-02-0.

Matrix Photochemistry of (η^5-Cyclopentadienyl)bis(ethene)rhodium and (η^5-Cyclopentadienyl)(ethene)carbonylrhodium: A Test-Bed for Intermediates in C–H Activation

David M. Haddleton,† Andrew McCamley, and Robin N. Perutz*

Contribution from the Department of Chemistry, University of York, York YO1 5DD, U.K.
Received July 1, 1987

Abstract: The photochemical reactivities of $CpRh(C_2H_4)_2$ (**1**) and $CpRh(C_2H_4)CO$ (**2**) ($Cp = \eta^5\text{-}C_5H_5$) have been examined in low-temperature matrices with IR and UV/vis detection. Photodissociation of ethene from **1** in inert matrices (Ar or CH_4) yields the coordinatively unsaturated $CpRh(C_2H_4)$; the reaction is reversed by long-wavelength irradiation. The identity of $CpRh(C_2H_4)$ is demonstrated with ^2H labeling of ethene and cyclopentadienyl groups. The IR results support a "bent", ground-state geometry for $CpRh(C_2H_4)$. UV photolysis of **1** in CO matrices releases ethene and generates **2** and $CpRh(CO)_2$ sequentially. The corresponding reaction in nitrogen matrices leads to $CpRh(C_2H_4)(N_2)$. On photolysis of **1** in CO-doped methane matrices, $CpRh(CO)(CH_3)H$ is formed in addition to substitution products. Complex **2** undergoes loss of either CO, yielding $CpRh(C_2H_4)$, or of C_2H_4, yielding CpRhCO, on UV photolysis in argon matrices. These reactions are reversed by long-wavelength photolysis, but in more concentrated matrices $Cp_2Rh_2(CO)_2$ is formed as an additional product. In nitrogen matrices both $CpRh(C_2H_4)(N_2)$ and $CpRh(CO)(N_2)$ are generated. In methane matrices $CpRh(C_2H_4)$ is still detected on UV photolysis, but CpRhCO is replaced by the product of oxidative addition of methane, $CpRh(CO)(CH_3)H$. Long-wavelength photolysis removes $CpRh(C_2H_4)$ but increases conversion to the (methyl)hydride complex. These experiments demonstrate that oxidative addition of methane must proceed via CpRhCO. The role of CpRhL (L = C_2H_4, CO) intermediates in solution reactions is discussed.

Some of the most successful of recent C–H activation reactions are thought to involve the dissociation of a small molecule from organometallic rhodium and iridium complexes in the primary step. Photochemical reactions of ($\eta^5\text{-}C_5R_5$)MLH_2 and ($\eta^5\text{-}C_5R_5$)ML_2 and thermal reactions of ($\eta^5\text{-}C_5R_5$)ML(H)R′ species (R = H, Me; R′ = alkyl; L = CO, phosphine, etc.; M = Rh, Ir) with alkanes have recently been postulated to proceed through ($\eta^5\text{-}C_5R_5$)ML, 16-electron intermediates.[1,2] Such fragments have excited considerable theoretical interest because of their carbenoid character and because both triplet and singlet states are available to them.[3] Attempts have been made to calculate the (ring-centroid)ML angle of the fragment and its dependence on spin state and to define those factors that stabilize the singlet state relative to the triplet.[3] However, experimental observation of these fragments has been extremely limited.

Photochemical matrix-isolation experiments on $Cp^*Ir(CO)_2$ ($Cp^* = \eta^5\text{-}C_5Me_5$) failed to induce CO loss in inert matrices, probably because of in-cage recombination. This conclusion has been confirmed in detailed studies of ($\eta^5\text{-}C_5R_5$)$M(CO)_2$ by Rest

* Author to whom correspondence should be addressed. No reprints available.

† Present address: Department of Chemistry, University of Southern Mississippi, Hattiesburg, MS 39406.

(1) (a) Janowicz, A. H.; Bergman, R. G. *J. Am. Chem. Soc.* **1982**, *104*, 352. (b) Janowicz, A. H.; Bergman, R. G. *Ibid.* **1983**, *105*, 3929. (c) Periana, R. A.; Bergman, R. G. *Organometallics* **1984**, *3*, 508. (d) Bergman, R. G.; Seidler, P. F.; Wenzel, T. T. *J. Am. Chem. Soc.* **1985**, *107*, 4358. (e) Stoutland, P. O.; Bergman, R. G. *Ibid.* **1985**, *107*, 4581. (f) Buchanan, J. M.; Stryker, J. M.; Bergman, R. G. *Ibid.* **1986**, *108*, 1537. (g) Periana, R. A.; Bergman, R. G. *Ibid.* **1986**, *108*, 7332. (h) Jones, W. D.; Feher, F. J. *Ibid.* **1982**, *104*, 4240. (i) Jones, W. D.; Feher, F. J. *Ibid.* **1984**, *106*, 1650. (j) Jones, W. D.; Feher, F. J. *Ibid.* **1985**, *107*, 620. (k) Hoyano, J. K.; McMaster, A. D.; Graham, W. A. G. *Ibid.* **1983**, *105*, 7190.

(2) Crabtree, R. H. *Chem. Rev.* **1985**, *85*, 245.

(3) (a) Hoffman, P.; Padmanabhan, M. *Organometallics* **1983**, *2*, 1273. (b) Dedieu, A.; Veillard, A. *Theor. Chim. Acta* **1983**, *63*, 339. (c) Silvestre, J.; Calhorda, M. J.; Hoffmann, R.; Stoutland, P. O.; Bergman, R. G. *Organometallics* **1986**, *5*, 1841.

0002-7863/88/1510-1810$01.50/0